MS_2 (M = Co and Ni) Hollow Spheres with Tunable Interiors for High-Performance Supercapacitors and Photovoltaics

Shengjie Peng, Linlin Li, Huiteng Tan, Ren Cai, Wenhui Shi, Chengchao Li, Subodh G. Mhaisalkar, Madhavi Srinivasan, Seeram Ramakrishna,* and Qingyu Yan**

We demonstrate in this paper facile synthesis of CoS_2 and NiS_2 hollow spheres with various interiors through a solution-based route. The obtained CoS_2 microspheres constructed by nanosheets display a three-dimensional architecture with solid, yolk-shell, double-shell, and hollow interiors respectively, with continuous changes in specific surface areas and pore-size distributions. Especially, the CoS_2 hollow spheres demonstrate excellent supercapacitive performance including high specific capacitance, good charge/discharge stability and long-term cycling life, owing to the greatly improved faradaic redox reaction and mass transfer. Furthermore, CoS_2 hollow spheres exhibit superior electrocatalytic activity for disulfide/thiolate (T_2/T^-) redox electrolyte in dye-sensitized solar cells (DSCs). Therefore, this work provides a promising approach for the design and synthesis of structure tunable materials with largely enhanced supercapacitor behavior, which can be potentially applied in energy storage devices.

1. Introduction

Over the last two decades, transition metal chalcogenides have attracted much attention, due to their excellent optical, electrical, magnetic and catalytic properties.[1–4] These unique properties can lead to wide applications in supercapacitors, lithium-ion batteries, DSCs, et al.[5–11] As important transition metal sulfides, CoS_2 showed high capacitances in electrochemical capacitors, due to their high redox activity. In addition, CoS_2 has been demonstrated to be very effective in catalyzing redox electrolytes in DSCs, showing a potential replacement for the noble metal Pt counter electrodes to lower the cost of the DSCs. These superior performances make metal sulfides, especially CoS_2, promising in the applications of supercapacitors and DSCs. Stimulated by the attractive properties and promising applications, several methods have been developed to prepare MS_2 (M = Co and Ni) materials with a wide range of nanostructures, including ellipsoids, microspheres, microtubes and microflowers.[12–17] However, there is still much room for progress with regard to the development of MS_2 nanostructures with different morphologies and their energy applications.

Recently, extensive attention has been paid to three-dimensional (3D) hollow nanostructures because of their attractive properties of low density, high surface-to-volume ratio, and low coefficients of thermal expansion, which make them promising in the applications of energy.[18,19] Especially for supercapacitors, hollow structures with high surface areas and suitable mesopores (especially 2–5 nm) can provide rich electroactive sites and short diffusion paths for charge carriers, which are required in the Faradaic redox reactions.[20,21] As for DSCs, the photovoltaic conversion efficiency can be improved by using counter electrodes with high surface areas. Thus, the porous hollow structure with a high surface area can lead to high catalytic activity for redox electrolytes and fast reaction rate.[22,23] Furthermore, two-dimensional nanosheet structures have the advantages of enhancing the effective interaction between the active materials and electrolytes and reducing transport lengths for both mass and charge transport.[24,25] Up to now, a variety of hollow structures with different complex interiors, such as core-shell, yolk-shell, and multi-shell structures, have been successfully fabricated mainly through hard and soft template-assisted approaches.[26–28] As compared to the much more common hard-template techniques, soft templates can be easily removed by gentle evaporation or dissolution in solvents. To the best of our knowledge, systematic study for the fabrication of CoS_2 and NiS_2 hollow structures with various interiors constructed by nanosheets are rarely reported. Therefore, it is highly desirable but challenging to synthesize MS_2 (M= Co, Ni) hollow structures and investigate their applications in supercapacitors and DSCs.

Dr. S. Peng, L. Li, H. Tan, R. Cai, W. Shi, C. Li, Prof. S. G. Mhaisalkar, M. Srinivasan, Q. Yan
School of Materials Science and Engineering
Nanyang Technological University
Singapore, 639798
E-mail: sjpeng@ntu.edu.sg; alexyan@ntu.edu.sg
Dr. L. Li, H. Tan, W. Shi, Prof. M. Srinivasan, Q. Yan
TUM-CREATE Center for Electromobility
Nanyang Technological University
62 Nanyang Drive, Singapore, 637459
Prof. S. Ramakrishna
Centre for Nanofibers and Nanotechnology
National University of Singapore
Singapore, 117576
E-mail: seeram@nus.edu.sg

DOI: 10.1002/adfm.201303273

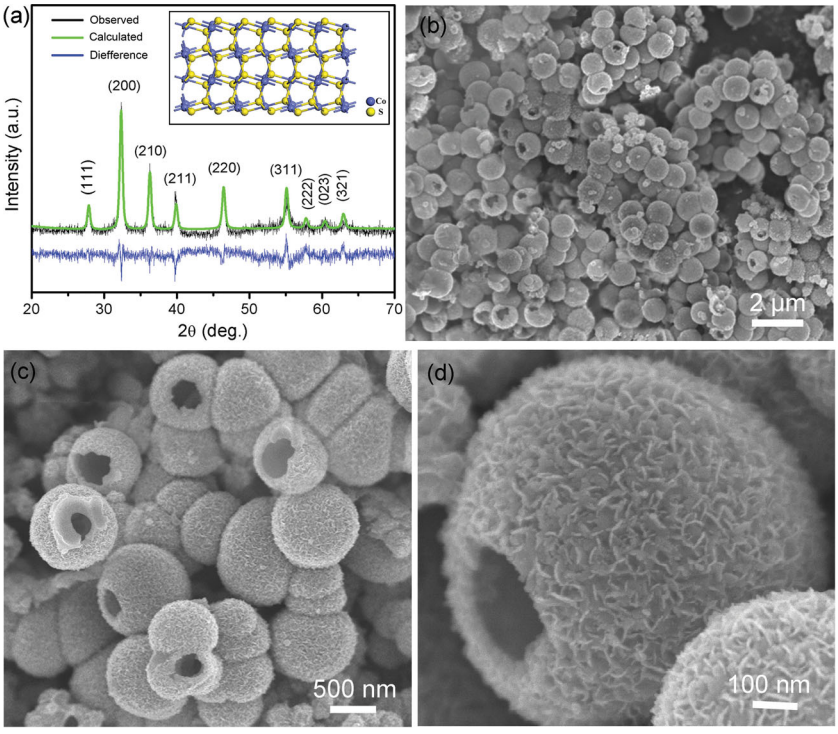

Figure 1. Rietveld refined XRD pattern (a) and SEM images (b, c, and d) of the CoS_2 hollow spheres. The inset of (a) is the corresponding crystal structure.

In the present study, we report facile synthesis of CoS_2 and NiS_2 hollow structures with tunable interiors through a facile solution-based method. It is found that the interior structures can be tuned from solid, yolk-shell and double-shell to hollow structures by using different amounts of CS_2. In the reaction system, the CS_2 oil droplets evaporation and self-assembly crystallization mechanism is proposed to account for the formation of nanosheet-constructed microspheres with various interiors. The obtained CoS_2 hollow spheres with the highest surface area and a mesopore distribution (2–5 nm) demonstrate superior performances in supercapacitors and DSCs. As supercapacitor electrodes, CoS_2 hollow spheres depict specific capacitances of 1301 and 450 F g^{-1} at current densities of 1 and 20 A g^{-1}, respectively. When used as the counter electrode, the CoS_2 hollow spheres demonstrate superior electrocatalytic activity for the organic T_2/T^- redox electrolyte in DSCs, which is higher than the conventional Pt electrodes.

2. Results and Discussion

The phase and purity of the product are analyzed by X-ray diffraction (XRD) (**Figure 1**a). The crystal structure of the hollow spheres was refined against powder XRD data using the Rietveld method. The cell parameters can be determined to be a = 5.512 Å, corresponding well with cubic CoS_2 (JCPDS No. 41-1471). No peak from impurity phase can be detected in the XRD pattern. The crystal structure of cubic CoS_2 is demonstrated in the inset of Figure 1. The scanning electron microscopy (SEM) images in Figure 1b-c reveal that the product is highly uniform spheres with an average size of about 800 nm. Some of the shells are partially broken (Figure 1c), clearly demonstrating the hollow nature of the as-prepared spheres. The spheres show rough surface and are composed of sheet-like subunits (Figure 1d).

The transmission electron microscopy (TEM) images in **Figure 2**a–c further confirm that the sample is hollow spheres composed of nanosheets. The wall thickness of the hollow spheres is about 180 nm (Figure 2b). Figure 2c shows that the nanosheet subunits is thin (e.g., ~5 nm in thickness), as highlighted by the arrows. The HRTEM image in Figure 2d reveals that the observed lattice interplanar spacings of around 0.322 and

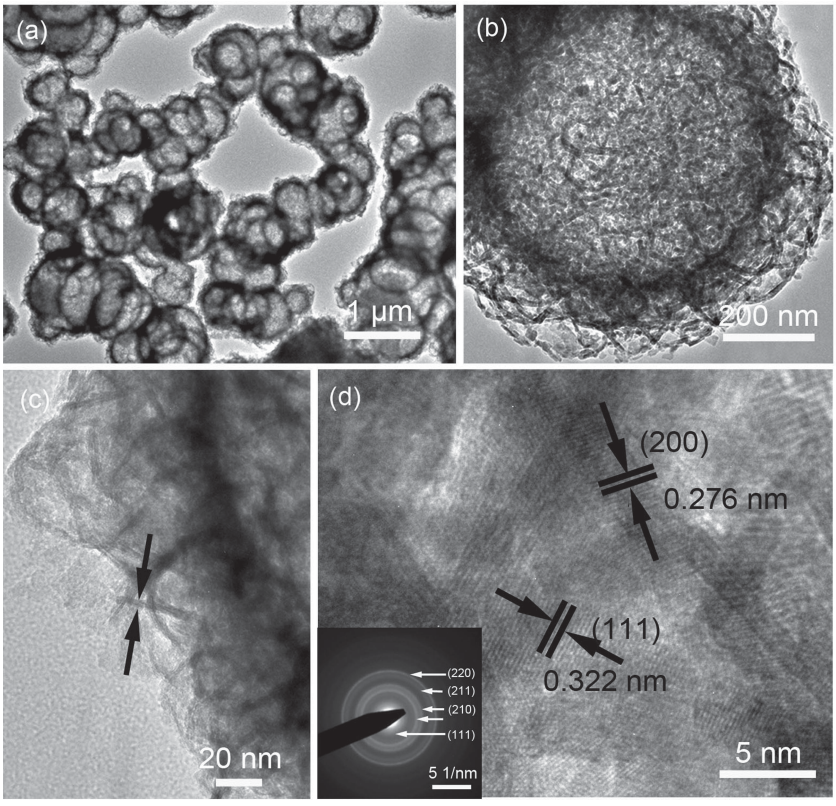

Figure 2. TEM (a–c), HRTEM (d) images and the SAED image (inset) of CoS_2 hollow spheres.

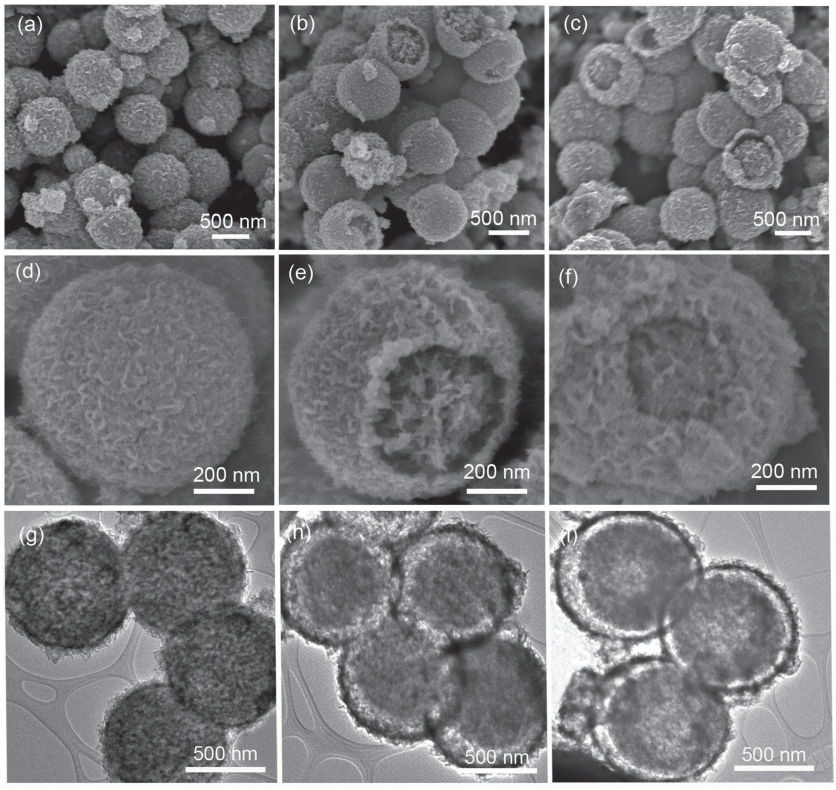

Figure 3. SEM (a–f) and TEM images (g–i) of solid, yolk-shell and double-shell CoS_2 spheres obtained by using different amounts of CS_2: 0.3 mL (a, d, and g), 0.4 mL (b, e, and h), and 0.5 mL (c, f, and i).

0.276 nm correspond to the distances of (111) and (200) planes of cubic CoS_2, respectively. And the ring pattern of the selected area electron diffraction (SAED) (inset in Figure 2d) demonstrates the polycrystalline of the CoS_2.

It is known that the amount of the CS_2 oil droplets has an important effect on the morphology of the product.[29,30] We thus collected samples prepared by using 0.3 mL, 0.4 mL, and 0.5 mL, respectively. All these as-collected samples are found to be CoS_2, as confirmed by the XRD results (Figure S1 in the Supporting Information). **Figure 3** shows the SEM and TEM images of the three samples. When only 0.3 mL of CS_2 is added into the system, the sample shown in **Figure 4**a,d,g presents nanospheres of about 800 nm in diameter, with no internal void space. The surface of the microspheres is composed of nanosheets. No obvious difference between the edge and the central parts in the TEM image further confirms their solid nature. When 0.4 mL of CS_2 is used, the product is yolk-shell spheres with an average diameter of 800 nm (Figure 3b,e,h). And the interior core with a size of about 300 nm presents mostly intact. It is found that both of the core and shell are constructed by nanosheets. A gap distance of about 100–200 nm is clearly observed between the core and the shell. When the amount of CS_2 increases to 0.5 mL, the product presents large spheres with a diameter of ~800 nm (Figure 3c,f,i). These 800-nm spheres are double-shelled structure and the gap between two shells is about 100–300 nm. The thickness of the outer shell is similar to the sample obtained by using 0.4 mL of CS_2, while the interior part is composed of a core-shell structure with a hollow part of 200 nm. After adding 0.8 mL of CS_2, the microspheres eventually evolve into completely hollow spheres with a diameter of about 800 nm and a shell thickness of about 50 nm.

It is found that the morphology can also be significantly affected by using different amounts of ethylenediamine (EN) in the reaction system. The purity and morphology of the products by using different amounts of EN (0 mL, 0.1 mL, 0.2 mL, and 0.3 mL) are analyzed by XRD and SEM (Figure S2 and S3 in the Supporting Information). The XRD patterns indicate that all the products are CoS_2. The sample obtained without using EN presents nanoparticle aggregates without any regular morphology. When using 0.1 mL of EN, the product is composed of small nanoparticles and nanoplates. With the increase of EN to 0.2 mL, the nanoparticles aggregate with each other to form nanospheres, and some nanoplates insert the nanospheres. Furthermore, several hollow nanospheres can be observed in the product. When 0.3 mL of EN is used, spheres with a size of about 800 nm are obtained and several spheres present hollow structures. The hollow spheres are constructed by nanosheets, which is similar to the product obtained by using 0.5 mL EN. The result shows that the product can evolve from nanopaticles, nanoplates, and hollow spheres with the increase of EN, further indicating the importance of a certain amount of EN in the formation of hollow structures composed of nanosheets.

The surface area and pore-size distribution are important keys for the electroactive materials in supercapacitors. Therefore, the solid, yolk-shell, double-shell, hollow CoS_2 spheres

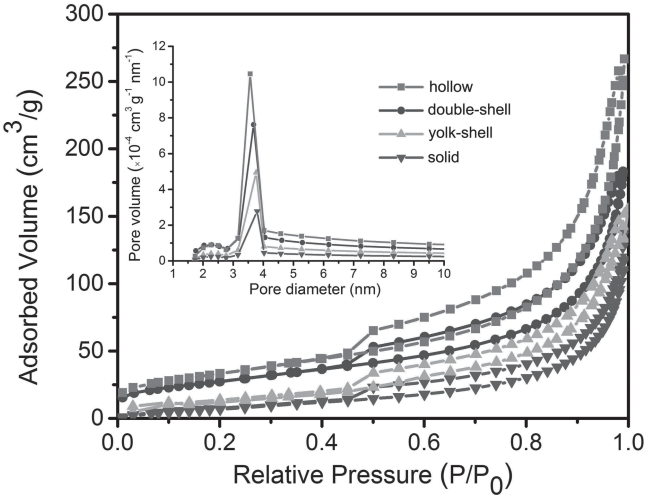

Figure 4. N_2-sorption isotherms and pore size distribution (inset) of solid, yolk-shell, double-shell and hollow CoS_2 spheres.

and CoS_2 bulk are investigated for their surface areas and porosity properties by N_2 adsorption/desorption isotherm (Figure 4). They all displays a type-IV isotherm with a type-H3 hysteresis loop in the relative pressure range of 0.5–1.0 p/p_0, indicating the presence of mesoporous structure.[31] Typically, the hollow spheres display narrow pore size distribution in the range of 2–5 nm (inset in Figure 4), which is calculated using the Barrett-Joyner-Halenda (BJH) method from the two branches of the isotherm. Furthermore, the specific surface area of hollow CoS_2 spheres is 127.6 $m^2\ g^{-1}$, which is larger than that of double-shell (98.3 $m^2\ g^{-1}$), yolk-shell (65.1 $m^2\ g^{-1}$) and solid (41.5 $m^2\ g^{-1}$) spheres. In contrast, the CoS_2 bulk no mesopores in the range 2–5 nm and only a low surface area of 3.2 $m^2\ g^{-1}$ (Figure S4 in the Supporting Information).

In the synthesis, the CoS_2 hollow spheres constructed by nanosheets can be obtained through a hydrothermal process by using soft templates. During the reaction, the Co^{2+}, EN, H_2O and CS_2 can form a similar oil/water system. EN can react with CS_2 to release H_2S at the oil-water interface and provide a sulfur source for the formation of CoS_2. The detailed reaction equation is described as follows.

$$Co(CH_3COO)_2 + EN \rightarrow [Co(EN)_3]^{2+} \quad (1)$$

$$H_2N(CH_2)_2NH_2 + CS_2 \rightarrow H_2N(CH_2)_2NH\text{-}CSSH \quad (2)$$

$$H_2N(CH_2)_2NH\text{-}CSSH \rightarrow [\text{-}HN(CH_2)_2NH\text{-}CS\text{-}]_n + H_2S \quad (3)$$

$$2[Co(EN)_3]^{2+} + 4H_2S + O_2 \rightarrow 2CoS_2 + 6EN + 2OH^- + 6H^+ \quad (4)$$

Based on the above experimental observations, a plausible formation mechanism of the nanosheet-assembled CoS_2 hollow spheres is proposed and shown in **Figure 5**. The formation process of CoS_2 hollow spheres mainly can be divided into two stages, including formation of EN-H_2O-CS_2 system and crystallization processes. Firstly, in the beginning, the functional group $-NH_2$ in the EN has a strong tendency to coordinate with Co^{2+} to form a stable $[Co(EN)_3]^{2+}$ complex, indicated by the formation of brown solution from the red Co^{2+} colour after introducing EN into the solution.[32] After adding CS_2 in the reaction system, CS_2 can mix with EN and water solvents to form a liquid-liquid heterogeneous solution under stirring a few minutes, resulting in the formation of a oil/water system. As the product of the reaction between CS_2 and EN has both hydrophobic and hydrophilic groups that can bridge the oil droplets and the water at the interface, this makes the oil droplets in the water stable at a certain condition. Therefore, a lot of nonpolar oil droplets (CS_2) are surrounded by hydrophilic group of the product of $[Co(EN)_3]^{2+}$ and water molecules, which prevent the droplets from agglomeration. And the CS_2 droplets can be used as the soft template. During the late stage of the hydrothermal process, the EN can carry Co^{2+} from the water phase to the oil-water interface. The EN reacts with CS_2 oil phase to release H_2S, which then reacts with Co^{2+} to form CoS_2 nuclei. In the experiment, the concentration of CoS_2 is high at the CS_2/water interface during the early stage. So the nanocrystals of CoS_2 may aggregate to form shell outside the unreacted CS_2 core. As the boiling point of CS_2 is low, the unreacted CS_2 cores may vaporize under the hydrothermal condition to leave the CoS_2 as hollow spheres. In the synthesis of binary transition metal sulfides with hydrothermal method, EN is the key factor to ensure the purity and morphology of the products. EN is known to be a strong chelating agent that can form a stable complex with metal ions, which may serve as molecular templates in control of the crystal growth.[33] It is believed that EN plays an important role in the growth process. The sample without using EN presents irregular bulk aggregates, which may be attributed to the fast reaction between Co^{2+} and S^{2-}. Here, the function of EN is to form a complex with Co^{2+} ions through a coordination interaction that controls the release rate of Co^{2+} from the complex, thus lowering the precipitation rate of CoS_2 and enhancing the product regularity. With the presence of EN, CS_2 can be enwrapped in the spheres formed by aggregation of CoS_2 nanocrystals. These nanocrystals are mostly sheet-like structures due to the capping of EN.

In the present system, the CS_2 plays roles not only as the oil droplets but also the sulfur source in the reaction. When a small amount of CS_2 is added into the reaction, the reaction would consume all the CS_2 and no surplus CS_2 oil droplets form. Therefore, only solid microspheres can be obtained when using a small amount of CS_2. After adding more CS_2, these CS_2 moleculars can aggregate and form more oil droplets. When the reaction starts, some CoS_2 nanoparticles aggregate to form small spheres (core), consuming

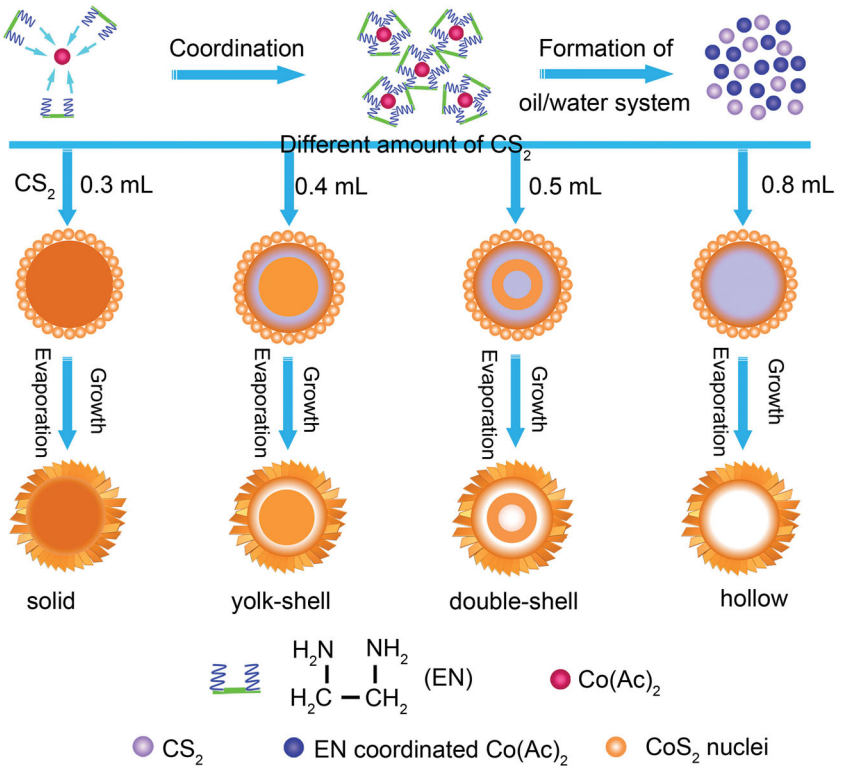

Figure 5. The schematic illustration of the formation process of different structured CoS_2: solid, yolk-shell, double-shell, and hollow spheres.

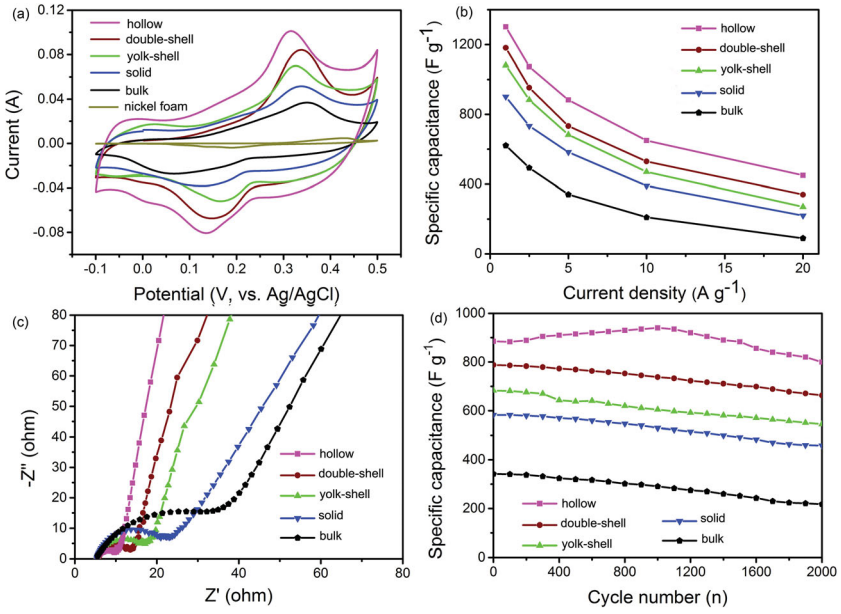

Figure 6. Cyclic voltammogram curves at a current density of 30 mV s^{-1} (a), specific capacitance as a function of current density (b), and Nyquist plots of the EIS (c) for the solid, yolk-shell, double-shell, hollow CoS_2 spheres and CoS_2 bulk, respectively; and specific capacitance and coulombic efficiency vs. cycle number at a current density of 5.0 A g^{-1} for the CoS_2 hollow spheres (d).

some oil droplets. Simultaneously, some CoS_2 nanoparticles can recrystallize to form nanosheets, dispersing outside the oil droplets (shell). Then these oil droplets may evaporate and uniform spheres with yolk-shell, and double-shell structures can be obtained. In addition, this method can be readily extended to the fabrication of other sulfides microspheres by changing the metal salt precursors. To further demonstrate the versatility of this method, we extended the synthesis to prepare with various interiors. The example of NiS_2 hollow spheres with tunable interior structure is shown in Figure S5, S6 and S7 in the Supporting Information, demonstrating the feasibility and generality of this approach in controlling the morphology of CoS_2 materials.

The electrochemical properties of the CoS_2 samples were further evaluated. **Figure 6**a shows the cyclic voltammetry (CV) of the CoS_2 hollow spheres with various interiors in 2 M KOH solution at a current density of 30 mV s^{-1}. All curves exhibit a similar shape and the shape of the CV curves suggests typical pseudocapacitive characteristics. The electrochemical reversible electron transfer process mainly involves the changes of the Co^{2+}/Co^{3+} redox couple, and mediated by the OH^- ions in the alkaline electrolyte.[34] A higher current density for the hollow spheres indicates a higher pseudocapacitance.[35] It should be noted that the current density generated by the nickel foam is very low based on the CV areas, as compared with that of the active material. Therefore, the capacitance is mainly attributed to the CoS_2 material.

To further evaluate the potential application of the CoS_2 hollow structure with various interiors as electrodes for supercapacitors, galvanostatic charge-discharge measurements were carried out in a 2 M KOH electrolyte at various current densities ranging from 1 to 20 A g^{-1} (Figure S8 in the Supporting Information). The specific capacitances of the hollow spheres electrode can be calculated based on the charge-discharge curves and the results are plotted in Figure 6b. Encouragingly, the CoS_2 hollow sphere electrode exhibits high pseudocapacitance of 1301, 1073, 883, 650 and 450 F g^{-1} at current densities of 1, 2.5, 5, 10 and 20 A g^{-1}, respectively. As a comparison, we also tested the specific capacitance of electrode made from bulk CoS_2 and other CoS_2 spheres. The corresponding specific capacitance is 735, 524, 406, and 177 F g^{-1} at a current density of 5 A g^{-1} for the hollow, double-shell, yolk-shell microspheres and CoS_2 bulk, respectively, which further confirms the highest specific capacitance of the hollow sample. Such superior pseudocapacitive performance is rarely observed for electroactive CoS_2. The high pseudocapacitive performance is attributed to the advantageous structural features. The ultrathin nanosheets construct the mesoporous spheres, which give rise to very high surface area and provide numerous electroactive sites for redox reaction. Moreover, the open space between these ultrathin nanosheets and abundant mesopores existing in the nanosheets can sever as a robust reservoir for ions, and greatly shorten the diffusion paths within the electrode.[36,37]

The superior electrochemical performance of the hollow microspheres was further confirmed by the electrochemical impedance spectroscopy (EIS) measurements. Figure 6c shows the Nyquist plots of the EIS spectra for hollow, double-shell, solid, and CoS_2 bulk respectively. The semicircle diameter of EIS equals the electron transfer resistance, which controls the electron transfer kinetics of the redox Co^{2+}/Co^{3+} couple at the electrode interface. It is found that the hollow electrode shows much smaller radius of semicircle in the Nyquist plots as compared to those of other CoS_2 spheres and bulk electrodes. The results are in high agreement with their CV, which clearly demonstrate that the hollow structure possesses lower resistance and thus allows for much faster electron transfer. The lower resistance of the hollow CoS_2 microspheres indicates a faster electron transfer between the active material and the charge collector. This is probably due to the higher specific surface area of the hollow microspheres compared with other CoS_2 samples, which facilitates the effective exposure of active sites.

It is well-accepted that long-term cycling performance is an important requirement for supercapacitors applications. Figure 6d shows the specific capacitances versus cycle number for the CoS_2 hollow spheres at a current density of 5 A g^{-1}. It can be observed that about 90.1% of specific capacitance can be retained after 2000 cycles, demonstrating the good long-term electrochemical stability of CoS_2 hollow spheres. The capacitance for the hollow CoS_2 spheres increases gradually up to 940 F g^{-1} during the initial 1000 cycles, which can be attributed to the full activation of the present electrode.[38] However, the CoS_2 bulk show the worst cycling stability (30.2% loss), possibly resulting from the compact particles, which are detrimental

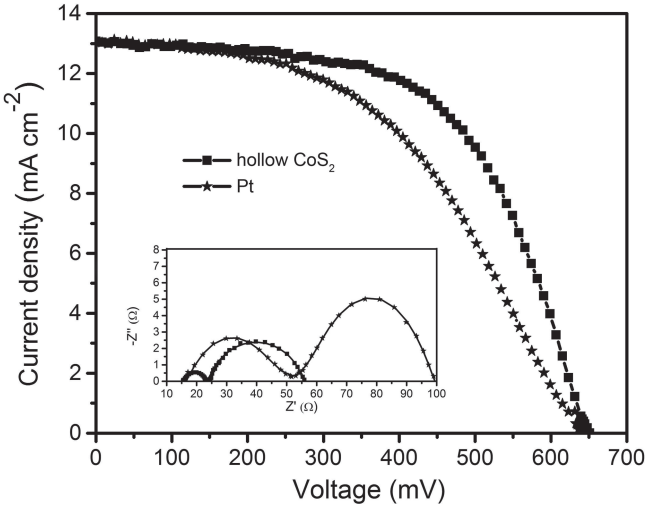

Figure 7. Current density–voltage (*J–V*) curves of the DSCs assembled by CoS_2 hollow spheres and Pt electrodes, respectively. The inset is the EIS Nyquist plots of the symmetrical cells consisting of two identical electrodes.

to electrolyte transport and active site accessibility during the cycling process. The large surface area and optimal pore-size of the hollow microspheres guarantee the high specific capacitance and good cycle stability. However, it should be noted that after prolonged charge-discharge cycling, some of the CoS_2 hollow spheres will be collapsed because of the ultrathin nanosheet shell structure, leading to a certain amount of capacitive decay (Figure S9 in the Supporting Information).

The CoS_2 hollow spheres were also tested as a catalyst in counter electrodes (CEs) for DSCs based on T_2/T^- electrolyte. Due to metal corrosion and visible light absorption properties of I_3^-/I^- redox couple, great interest has been focused on organic thiolate/disulfide redox couples.[27,39] **Figure 7** shows the photovoltaic performance of the DSCs based on CoS_2 hollow spheres and Pt electrodes under standard simulated AM 1.5 illumination at 100 mW cm^{-2}. CoS_2 hollow spheres exhibit a short-circuit photocurrent density (J_{sc}) of 12.88 mA cm^{-2}, open-circuit photovoltage (V_{oc}) of 641 mV, and fill factor (*FF*) of 59.3%, yielding overall conversion efficiency (η) of 4.89%, which is higher than the conventional Pt-based DSC (4.00%).

With respect to photovoltaic performance, it is found that the biggest varied performance parameter is the *FF* value. Therefore, electrochemical impedance spectroscopy (EIS) measurement was carried out to study the charge-transfer process at the interface between the different electrodes and the electrolytes. The inset of Figure 7 shows EIS curves of dummy cells constructed by two identical CEs. Two semicircles are clearly observed. The semicircles in high and low frequency range are assigned to the impedance related to the charge-transfer processes occurring at the CE/electrolyte interface and the Nernst diffusion impedance within the electrolyte, respectively. It is known that the charge transfer resistance (R_{ct}) (high-frequency semicircle) represents the catalytic performance for I_3^- reduction.[40] The smaller the semicircle is, the better the catalytic performance is. The R_{ct} (8.2 Ω) of the CoS_2 electrode is lower that the Pt electrode (36.5 Ω). This indicates that the CoS_2 hollow spheres are more suitable for the T_2/T^- electrolyte, compared to the conventional Pt electrodes. As is known, the derived charge transfer resistances for the different electroactive materials are correlated with the fill factors and the final power conversion efficiencies.[41,42] A smaller R_{ct} value suggests higher catalytic activity. Furthermore, the CoS_2-based DSC shows a better photoelectrical response, and its absolute incident photon-to-current conversion efficiency (IPCE) is higher than that of Pt-based DSC over the entire wavelength region of 400–800 nm (Figure S10 in the Supporting Information). This is also in good agreement with the observed higher J_{sc} of CoS_2-based DSC. Therefore, compared to the Pt electrode, the higher catalytic activity of CoS_2 hollow spheres in the T_2/T^- electrolyte leads to higher conversion efficiency. The stability of the DSCs was primarily tested (Figure S11 in the Supporting Information). It is found that the CoS_2-based DSC maintained about 71% of their initial performance when being stored in the dark for 25 days, which is higher than the Pt-based DSC (45%). The performance result indicates that the CoS_2 hollow spheres may be a promising candidate as counter electrodes (CEs) for the DSCs by using T_2/T^- electrolytes.

3. Conclusions

We have developed simple hydrothermal synthesis of CoS_2 and NiS_2 hollow spheres with tunable interiors. The growth process of CoS_2 hollow spheres goes through CS_2 oil droplets evaporation and self-assembly crystallization processes. The hollow CoS_2 spheres exhibit excellent pseudocapacitance performance, including high specific capacitance, good charge/discharge stability and long-term cycling life, superior to the solid, yolk–shell, and double-shell structures and bulk counterparts. This can be ascribed to the specific 3D architecture with enhanced surface area and suitable mesopore distribution, which improves the faradic redox reaction and benefits the mass transfer of electrolytes. Furthermore, the hollow CoS_2 spheres exhibit superior electrocatalytic activity for T_2/T^- redox electrolyte in DSCs. It is expected that the approach for tuning the interior structures of CoS_2 microspheres can be extended to other sulfides for the purpose of obtaining largely enhanced physiochemical property.

4. Experimental Section

Synthesis of CoS_2 and NiS_2: In a typical synthesis of CoS_2 hollow nanospheres, 2 mmol (0.498 g) of $Co(CH_3COO)_2 \cdot 4H_2O$, and 35 mL of distilled water were loaded into a Teflon-lined stainless steel autoclave with 50 mL capacity and stirred for 10 min to form a red solution. Then 0.5 mL of EN was dropped into the solution and the solution changed from red to dark green after 20 min stirring. Finally, 0.8 mL of CS_2 as a sulfur source was added into the solution and stirred for another 20 min. After that, the autoclave was sealed, maintained at 200 °C for 18 h, and cooled naturally to room temperature. The as-derived powder was washed by deionized water several times and dried at vacuum at 80 °C for 12 h. Moreover, different samples were also prepared with different amounts of CS_2 of EN to study the amount effect on the structures and the morphologies of the CoS_2 hollow spheres. As an extended method, NiS_2 hollow structures can be obtained by using 0.5 mL EN, 1 mL CS_2 and corresponding metal salts $Ni(NO_3)_2 \cdot 6H_2O$ at 180 °C for 12 h, respectively.

Materials Characterization: The phase purity and the structure of the as-prepared products were determined by XRD with Cu Kα

radiation (λ = 1.5418 Å) at a scan rate of 0.04° s^{-1}. The morphologies of the products were characterized by field-emission scanning electron microscopy (FESEM, JEOL, JSM-7600F) at an acceleration voltage of 5 kV. TEM and HRTEM were performed on a JEOL 2100F microscope with an accelerating voltage of 200 kV. EDX is attached on the TEM. The nitrogen adsorption-desorption isotherm and Barrett-Joyner-Halenda (BJH) methods were analyzed on a Micromeritics ASAP 2010 analyzer (accelerated surface area and porosimetry system).

Electrochemical Measurements: The working electrode was prepared by mixing 70 wt% of active material 20 wt% of Super P carbon (Timcal), and 10 wt% of polyvinylidene difluoride (PVDF, Kynar 2801)). This mixture was then coated on the Ni foam electrode and dried at 80 °C for 12 h. The electrochemical properties and capacitance measurements of the supercapacitor electrodes were investigated in a three-electrode half-cell system in 2 M KOH aqueous electrolyte with Solartron analytical equipment (Model 1470E). A platinum electrode and a standard calomel electrode were used as the counter electrode (SCE) and the reference electrode, respectively.

DSCs Fabrication and Measurements: The counter electrodes were prepared by adding several drops of the CoS_2 hollow structures dispersed in ethanol and Triton X-100 solution on the cleaned FTO substrates. A CoS_2 solution was prepared by adding 40 mg CoS_2 hollow spheres into 10 mL ethanol and 0.1 g Triton X-100 and then sonicated for 30 min to from a homogeneous solution. The CoS_2 films coating on FTO glass was then annealed in Ar at 350 °C for 30 min to obtain CoS_2 counter electrodes. TiO_2 electrodes were fabricated by coating the TiO_2 paste on the FTO substrates using a screen-printing and then doctor blade methods. The obtained TiO_2 films were dipped into the N719 acetonitrile solution for 24 h. DSCs were fabricated by sealing the electrolyte between the dye-sensitized TiO_2 electrodes and the counter electrodes with a 50 µm spacer. The electrolyte is di-5-(1-methyltetrazole) disulfide/5-mercapto-1-methyltetrazole N-tetramethylammonium salt (T_2/T^-), which contains 0.4 M $Me_4N^+T^-$, 0.4 M di-5-(1-methyltetrazole) disulfide (T_2), 0.05 M $LiClO_4$, and 0.5 M TBP in 6:4 (v/v) acetonitrile/ethylene carbonate. As comparison, conventional Pt electrodes were prepared by sputtering.

Electrochemical impedance spectroscopy (EIS) of the counter electrodes was investigated by using the Autolab PGSTAT30 from 40 Hz to 1 M Hz with signal amplitude of 10 mV to determine their catalytic performance. For the EIS measurement, a symmetric cell configuration with two identical counter electrodes was assembled with the injection of the same electrolyte for the DSCs. EIS spectra were obtained at zero bias potential and 10 mV amplitude over the frequency range 0.01–10^5 Hz. The current density–voltage (*J–V*) curves of the assembled DSCs were performed using a solar simulator (San Ei, Japan) under 1 sun and at AM 1.5G condition. IPCE measurements were done using the standard kit from Oriel Instruments (model QE-PV-SI, Silicon detector, Newport Corporation, US). The level of standard irradiance (1 Sun conditions, 100 mW cm^{-2}) was set with a calibrated c-Si reference solar cell.

Supporting Information

Supporting Information is available from the Wiley Online Library or from the author.

Acknowledgements

The authors gratefully acknowledge A*STAR SERC grant 1021700144, Singapore National Research Foundation under CREATE program: EMobility in Megacities and MPA 23/04.15.03 RDP 020/10/113 grant.

Received: September 22, 2013
Revised: October 25, 2013
Published online: December 5, 2013

[1] X. F. Duan, Y. Huang, R. Agarwal, C. M. Lieber, *Nature* **2003**, *421*, 241.
[2] M. R. Gao, Y. F. Xu, J. Jiang, S. H. Yu, *Chem. Soc. Rev.* **2013**, *42*, 2986.
[3] J. Joo, H. B. Na, T. Yu, J. H. Yu, Y. W. Kim, F. X. Wu, J. Z. Zhang, T. Hyeon, *J. Am. Chem. Soc.* **2003**, *125*, 11100.
[4] Y. L. Liang, R. J. Feng, S. Q. Yang, H. Ma, J. Liang, J. Chen, *Adv. Mater.* **2011**, *23*, 640.
[5] H. C. Sun, D. Qin, S. Q. Huang, X. Z. Guo, D. M. Li, Y. H. Luo, Q. B. Meng, *Energy Environ. Sci.* **2011**, *4*, 2630.
[6] J. Xie, S. Y. Liu, G. S. Cao, T. J. Zhu, X. B. Zhao, *Nano Energy* **2013**, *2*, 49.
[7] S. W. Chou, J. Y. Lin, *J. Electrochem. Soc.* **2013**, *160*, D178.
[8] L. Zhang, H. B. Wu, X. W. Lou, *Chem. Commun.* **2012**, *48*, 6912.
[9] T. Zhu, H. B. Wu, Y. B. Wang, R. Xu, X. W. Lou, *Adv. Energy Mater.* **2012**, *2*, 1497.
[10] J. W. Seo, J. T. Jang, S. W. Park, C. Kim, B. Park, J. Cheon, *Adv. Mater.* **2008**, *20*, 4269.
[11] C. Y. Chen, Z. Y. Shih, Z. Yang, H. T. Chang, *J. Power Sources* **2012**, *215*, 43.
[12] Y. X. Zhou, H. B. Yao, Y. Wang, H. L. Liu, M. R. Gao, P. K. Shen, S. H. Yu, *Chem. Eur. J.* **2010**, *16*, 12000.
[13] X. C. Jiang, Y. Xie, J. Lu, L. Y. Zhu, W. He, Y. T. Qian, *Adv. Mater.* **2001**, *13*, 1278.
[14] Q. H. Wang, L. F. Jiao, Y. Han, H. M. Du, W. X. Peng, Q. N. Huan, D. W. Song, Y. C. Si, Y. J. Wang, H. T. Yuan, *J. Phys. Chem. C* **2011**, *115*, 8300.
[15] J. Y. Lin, J. H. Liao, S. W. Chou, *Electrochim. Acta* **2011**, *56*, 8818.
[16] Y. J. Feng, T. He, N. Alonso-Vante, *Chem. Mater.* **2008**, *20*, 26.
[17] C. W. Kung, H.W. Chen, C. Y. Lin, K. C. Huang, R. Vittal, K. C. Ho, *ACS Nano* **2012**, *6*, 7016.
[18] Z. Yang, C. Y. Chen, C. W. Liu, H. T. Chang, *Chem. Commun.* **2010**, *46*, 5485.
[19] L. Li, X. C. Yang, J. Z. Zhao, J. J. Gao, A. Hagfeldt, L. C. Sun, *J. Mater. Chem.* **2011**, *21*, 5573.
[20] D. N. Futaba, K. Hata, T. Yamada, T. Hiraoka, Y. Hayamizu, Y. Kakudate, O. Tanaike, H. Hatori, M. Yumura, S. Iijima, *Nat. Mater.* **2006**, *5*, 987.
[21] H. Zhou, D. Li, M. Hibino, I. Honma, *Angew. Chem. Int. Ed.* **2005**, *44*, 797.
[22] B. Liu, S. Wei, Y. Xing, D. Liu, Z. Shi, X. C. Liu, X. J. Sun, S. Y. Hou, Z. M. Su, *Chem. Eur. J.* **2010**, *16*, 6625.
[23] I. Jeong, C. Jo, A. Anthonysamy, J. M. Kim, E. Kang, J. Hwang, E. Ramasamy, S. W. Rhee, J. K. Kim, K. S. Ha, K. W. Jun, J. Lee, *ChemSusChem* **2013**, *6*, 299.
[24] C. Xu, Y. Zeng, X. H. Rui, N. Xiao, J. X. Zhu, W. Y. Zhang, J. Chen, W. L. Liu, H. T. Tan, H. H. Hng, Q. Y. Yan, *ACS Nano* **2012**, *6*, 4713.
[25] Y. M. Wu, Z. H. Wen, J. H. Li, *Adv. Mater.* **2011**, *23*, 1126.
[26] J. G. Yu, H. T. Guo, S. A. Davis, S. Mann, *Adv. Funct. Mater.* **2006**, *16*, 2035.
[27] M. K. Wang, N. Chamberl, L. Breau, J. E. Moser, R. Humphry-Baker, B. Marsan, S. M. Zakeeruddin, M. Grätzel, *Nat. Chem.* **2010**, *2*, 385.
[28] Z. X. Deng, L. B. Li, Y. D. Li, *Inorg. Chem.* **2003**, *42*, 2331.
[29] B. Li, Y. Xie, J. X. Huang, Y. T. Qian, *Adv. Mater.* **1999**, *11*, 1456.
[30] L. H. Ai, H. T. Yue, J. Jiang, *Nanoscale* **2012**, *4*, 5401.
[31] K. S. W. Sing, D. H. Everett, R. A. W. Haul, L. Moscou, R. A. Pierotti, J. Rouquerol, T. Siemieniewska, *Pure Appl. Chem.* **1985**, *57*, 603.
[32] E. Naujalis, J. Čepytė, A. Padarauskas, *Anal. Bioanal. Chem.* **2003**, *376*, 759.
[33] J. T. Sampanthar, H. C. Zeng, *J. Am. Chem. Soc.* **2002**, *124*, 6668.

[34] F. Tao, Y. Q. Zhao, G. Q. Zhang, H. L. Li, *Electrochem. Commun.* **2007**, *9*, 1282.
[35] H. Jiang, T. Zhao, C. Z. Li, J. Ma, *J. Mater. Chem.* **2011**, *21*, 3818.
[36] M. F. Shao, F. Y. Ning, Y. F. Zhao, J. W. Zhao, M. Wei, D. G. Evans, X. Duan, *Chem. Mater.* **2012**, *24*, 1192.
[37] Y. Y. Gao, S. L. Chen, D. X. Cao, G. L. Wang, J. L. Yin, *J. Power Sources* **2010**, *195*, 1757.
[38] H. Jiang, J. Ma, C. Z. Li, *Chem. Commun.* **2012**, *48*, 4465.
[39] M. X. Wu, X. Lin, Y. D. Wang, L. Wang, W. Guo, D. D. Qi, X. J. Peng, A. Hagfeldt, M. Grätzel, T. L. Ma, *J. Am. Chem. Soc.* **2012**, *134*, 3419.
[40] S. J. Peng, J. F. Shi, J. Pei, Y. L. Liang, F. Y. Cheng, J. Liang, J. Chen, *Nano Res.* **2009**, *2*, 484.
[41] M. X. Wu, T. L. Ma, *ChemSusChem* **2012**, *5*, 1343.
[42] K. C. Huang, Y. C. Wang, R. X. Dong, W. C. Tsai, K. W. Tsai, C. C. Wang, Y. H. Chen, R. Vittal, J. J. Lin, K. C. Ho, *J. Mater. Chem.* **2010**, *20*, 4067.